









RESEARCH ARTICLE | NOVEMBER 17 2025

Metalens-coupled terahertz NbN hot electron bolometer mixer

D. Ren ; J. R. G. Silva ; S. Cremasco ; Z. Zhao ; W. Ji; J. de Graaff ; A. J. L. Adam ;
J. R. Gao  



Appl. Phys. Lett. 127, 202601 (2025)

<https://doi.org/10.1063/5.0292184>



View
Online



Export
Citation

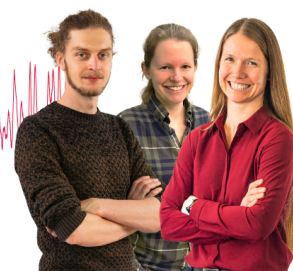
Webinar From Noise to Knowledge

May 13th – Register now



Zurich
Instruments

Universität
Konstanz



Metalens-coupled terahertz NbN hot electron bolometer mixer

Cite as: Appl. Phys. Lett. **127**, 202601 (2025); doi: [10.1063/5.0292184](https://doi.org/10.1063/5.0292184)

Submitted: 21 July 2025 · Accepted: 26 October 2025 ·

Published Online: 17 November 2025



View Online



Export Citation



CrossMark

D. Ren,¹ J. R. G. Silva,² S. Cremasco,¹ Z. Zhao,¹ W. Ji,¹ J. de Graaff,¹ A. J. L. Adam,¹ and J. R. Gao^{1,2,a)}

AFFILIATIONS

¹Department of Imaging Physics, Delft University of Technology, Lorentzweg 1, 2628 CJ Delft, The Netherlands

²Space Research Organization Netherlands (SRON), Niels Bohrweg 4, 2333 CA Leiden, and Landleven 12, 9747 AD Groningen, The Netherlands

^{a)}Author to whom correspondence should be addressed: j.r.gao@srn.nl

ABSTRACT

Enabled by planarized phase engineering, metalenses based on metasurfaces offer compact and scalable solutions for applications such as sensing, imaging, and virtual reality. They are particularly attractive for multi-pixel, large-scale heterodyne focal plane arrays in space observatories, where a flat metalens array on a silicon wafer can replace individual lenses, greatly simplifying system integration and beam alignment. In this work, we demonstrate a superconducting niobium nitride (NbN) hot electron bolometer (HEB) mixer coupled to a silicon-based metalens operating at terahertz frequencies. The metalens phase profile was derived from a finite-size Gaussian beam source using the Rayleigh–Sommerfeld diffraction integral, and its focusing behavior was validated through 2D simulation. Experimentally, the metalens-coupled NbN HEB receiver exhibited a noise temperature of 1800 K at 1.63 THz. The power coupling efficiency from free space to the mixer via the metalens was measured to be 25%. Measured far-field beam profiles are Gaussian-like with sidelobes below -14 dB. These results demonstrate the feasibility of integrating metalenses with HEB mixers for THz detection, offering a scalable path for compact focal plane arrays in space-based THz instrumentation.

Published under an exclusive license by AIP Publishing. <https://doi.org/10.1063/5.0292184>

Superconducting hot electron bolometer (HEB) mixers are the most sensitive heterodyne detectors in the terahertz (THz) regime, typically covering frequencies from 1 to 6 THz.^{1,2} HEB mixers based on niobium nitride (NbN) bridges have demonstrated near quantum-noise-limited performance,^{3,4} enabling the detection of extremely weak signals and providing high spectral resolution with $f/\Delta f \geq 10^6$, where f is the frequency. Heterodyne instruments based on HEB mixers are critical for space-based astronomy, enabling the detection of fine-structure atomic and molecular lines, along with their Doppler shifts, such as ionized carbon [CII] at 1.901 THz, atomic oxygen [OI] at 4.745 THz, water, and other key tracers in molecular clouds, star-forming regions, and galaxies. Such observations provide crucial insights into the physical conditions of the interstellar medium.⁵

Single-pixel NbN HEBs or small arrays have been deployed in space on the ESA *Herschel Space Observatory*,⁶ on an airborne platform of the *Stratospheric Observatory for Infrared Astronomy* (SOFIA),⁷ and on NASA balloon-borne THz observatories, including the *Stratospheric Terahertz Observatory* (STO2)⁸ and the *Galactic/Extragalactic Ultra-Long-Durable Balloon Spectroscopic Terahertz Observatory* (GUSTO).⁹

An NbN bridge, with submicrometer dimensions ($<0.5 \mu\text{m}$), requires efficient free-space coupling of radiation via either a lens-antenna⁹ or feedhorn-waveguide⁷ structure. In lens-antenna systems, an antireflection (AR)-coated elliptical silicon lens focuses a Gaussian beam into a diffraction-limited spot at the antenna, achieving a calculated coupling efficiency of 92% at 1.63 THz.⁴

The 8-pixel arrays used in GUSTO, assembled from individual elliptical lens-HEB mixer units into a common metal block, represent the state of the art.⁹ Such arrays enable large-area sky surveys, as mapping speed scales inversely with pixel count (assuming constant per-pixel sensitivity). However, scaling beyond eight pixels, for instance, toward 100, faces practical challenges due to the labor-intensive alignment and beam-pointing verification at 4.2 K, required for each pixel.¹⁰

We propose an alternative architecture for large HEB FPAs using a flat silicon metalens, as shown in Fig. 1(a), in place of elliptical lenses. In this approach, the FPA is formed by bonding two well-aligned silicon wafers: one with an array of metalenses, the other with an array of antenna-coupled HEBs. This requires only a single alignment step for the entire array. Unlike individually fabricated elliptical lenses,

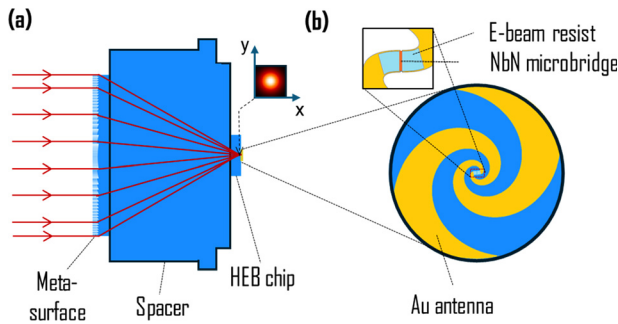


FIG. 1. (a) Schematic of a metalens-coupled HEB mixer, consisting of a metasurface, a disc-shaped spacer, and an HEB chip, all fabricated from silicon. The incident THz plane wave (red arrows) propagates toward the metasurface, which imparts spatially varying phase shifts across its aperture, converting the wave into a converging spherical wavefront focused onto the x - y plane where the HEB antenna is located, leading to a focused beam as illustrated. (b) Top view of the spiral antenna (yellow) on the HEB chip, with a zoomed-in view of the NbN microbridge at the center of the feed.

metalenses can be batch-fabricated using standard microfabrication processes, offering a compact, scalable, and cost-effective solution, similar to an approach pioneered for infrared FPAs.¹¹

Since the introduction of metasurfaces for wavefront control,¹² metalenses based on multilayer plasmonic or all-dielectric metasurfaces have been demonstrated across a broad spectral range.^{13–15} Numerous THz metalenses have been reported.^{16–19} For example, an all-dielectric metalens composed of rectangular silicon pillars achieved a theoretical focusing efficiency of 61.3% and a measured efficiency of 46% at 1 THz.¹⁹ Here, the focusing efficiency refers to the fraction of incident power concentrated at the focal spot. Plasmonic meta-atom approaches based on anisotropic metallic resonators in combination with a dielectric polyimide layer can also create an efficient flat lens operating over a wide frequency band ($\sim 40\%$), demonstrated at 400 GHz.¹⁴ However, so far no such flat lenses have been reported at frequencies above 1 THz, where Ohmic and dielectric losses, polarization conversion, and compatibility with detectors need to be examined.

We adopted the all-silicon design for several reasons: (1) silicon exhibits low loss at THz frequencies, allowing efficient transmission and phase control; (2) it provides excellent thermal and mechanical compatibility with the Si-based HEB chips, minimizing interface losses, simplifying fabrication, and improving alignment precision; and (3) it is fully compatible with cryogenic operation as required for a superconducting HEB.

To date, most THz metalens research has focused on free-space (air-to-air) light focusing. Although a silicon metalens integrated with an antenna-coupled transition-edge sensor bolometer has been proposed, it has only been explored through simulations.²⁰ No experimental demonstration of a metalens integrated with an antenna-coupled HEB has been reported.

In this work, we present an experimental demonstration of a metalens coupled to a NbN HEB mixer operating at 1.63 THz. Using standard heterodyne techniques, we measured the receiver noise temperature and evaluated the optical power coupling efficiency from the metalens to the HEB.

Figure 1(a) shows the schematic of the metalens-coupled HEB mixer. The structure consists of a Si micropillar-based metasurface on

a thin Si substrate, a thick Si spacer, and a thin Si HEB chip, together forming a configuration that resembles a solid-immersion lens. The spacer, in combination with the HEB chip substrate, extends the optical path length of the metasurface, allowing the beam to focus properly onto the spiral antenna integrated on the HEB chip. A superconducting NbN bolometer is positioned between the two antenna arms, as illustrated in Fig. 1(b), with the focal spot designed to coincide with the antenna center.

For simplicity, we refer to the metasurface sample as the “metalens” throughout the paper. The metalens has a diameter of 7.5 mm and a designed total length of 5115 μm in Si. These dimensions were chosen to fit an existing mixer block (see the [supplementary material 1](#)) used for heterodyne measurements. The individual thicknesses are: 515 μm for the metalens, 4220 μm for the spacer, and 380 μm for the HEB chip.

The metalens plane is defined at the interface between the metasurface and the silicon substrate, which is 215 μm from the air interface. This location is where the incident beam undergoes a phase change, resulting in a focal length of 4900 μm over a total propagation distance of 5115 μm . To derive the phase distribution of the electric field at the metalens plane, we use the Rayleigh–Sommerfeld diffraction integral to back-propagate a narrow source from the designed focal plane (x - y plane), leveraging the reciprocity of a lens, as illustrated in Fig. 1(a). The formula for the x -component (or y -component, depending on the spot polarization) of the electric field, $u(x, y, z)$, at the metalens plane is given by²¹

$$u(x, y, z) = -\frac{1}{2\pi} \iint_{-\infty}^{\infty} U(x_0, y_0) \cdot g(x - x_0, y - y_0, z, \lambda_0) dx_0 dy_0, \quad (1)$$

where the propagation kernel is $g(x, y, z, \lambda) = \exp(iknR) \cdot (ikn - 1/R) \cdot z/R^2$, $R^2 = x^2 + y^2 + z^2$, $k = 2\pi/\lambda$, n is the refractive index, λ is the wavelength, and $U(x_0, y_0)$ is the electrical field at the focal plane.

For this proof-of-concept demonstration, we selected a Gaussian beam source with a 100 μm waist, rather than optimizing for maximum focusing efficiency or perfect beam-mode matching to the antenna. A narrower source was avoided because our metalens design has a high numerical aperture (NA) of ~ 2 . High-NA designs inherently lead to smaller focal spots but often suffer from lower focusing efficiency, producing broader, less efficient beams that deviate from the target beam. This is due to diffraction from the flat lens structure, which can redirect light into unwanted zero- and higher-order back-ground modes.²²

To compute the scalar electric field, we used a refractive index $n = 3.384$ for Si at 4 K,²³ since the lens operates at cryogenic temperatures, and a wavelength λ_0 of 184.3 μm at 1.63 THz *in vacuo* and a wavelength in Si of 54.46 μm . Figure 2(a) shows the calculated phase distribution at the metalens plane, located 5020 μm from the HEB antenna. The phase profile exhibits a radially increasing gradient, indicating the need for finer spatial phase control near the lens edge to achieve accurate wavefront shaping. A focal length of 5020 μm was used to calculate the phase profile, rather than the target 4900 μm , to ensure the effective focus would occur at the intended antenna position of 5115 μm . This adjustment, suggested by 2D simulations using COMSOL Multiphysics® (COMSOL), to be presented later, accounts for a small focal shift likely caused by the finite aperture of the metalens (7.5 mm diameter) and its reduced efficiency in the outer region.

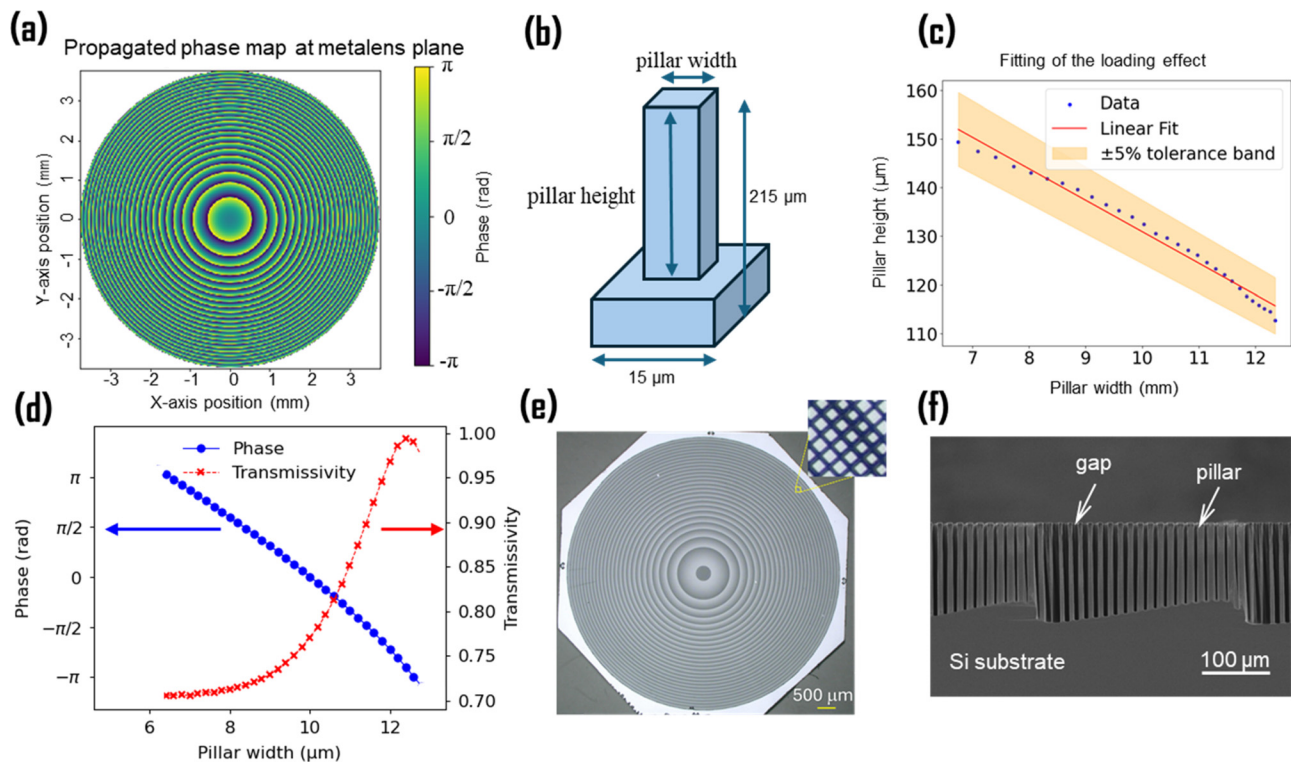


FIG. 2. (a) Simulated phase map at the metalens plane for focusing at 1.63 THz, showing concentric phase zones. (b) Schematic of a Si meta-atom unit with a lateral pitch of 15 μm and a total height of 215 μm , including both the pillar and part of the substrate. The pillar width varies, which also affects the achievable height, as shown in (c). (c) Measured pillar height as a function of width from a metalens. (d) Simulated phase shift (blue circles) and transmitted intensity vs square pillar width for 1.63 THz. (e) Optical micrograph of a fabricated Si metalens (with a slightly different phase map design than in (a)); inset: zoomed-in image illustrating Si pillars with bright squares. (f) SEM cross-sectional image showing high-aspect-ratio Si pillars and different heights.

To accommodate this high phase gradient, we adopt an all-Si metasurface approach following Ref. 19, using subwavelength meta-atoms with a 15 μm pitch. The meta-atoms consist of square Si pillars²⁴ with varying widths, as illustrated schematically in Fig. 2(b), to impart the required local phase shifts.

In principle, a constant pillar height could be assumed. However, in our metalens design, the pillar height varies with width due to fabrication constraints, as discussed in the fabrication section. Figure 2(c) shows the experimentally observed dependence, based on the pre-fabrication tests of a similar metalens. The pillar height ranges from 110 to 150 μm as the width decreases from 13 to 7 μm .

We employed the eigenmode solver in COMSOL to calculate the phase shift and transmission of meta-atoms for incident light at 1.63 THz by varying the pillar width from 7 to 13 μm . The corresponding pillar height was also varied, following the fitted linear relationship between width and height shown in Fig. 2(c). Figure 2(d) presents the calculated phase shift as a function of width, ranging from $-\pi$ to 1.0π , thereby achieving full $0-2\pi$ phase coverage. The simulated transmission varies between 70% and 100%.

The COMSOL simulations were performed using periodic boundary conditions with high-order diffraction modes enabled, allowing us to capture the grating-like behavior inherent to the periodic metalens structure.¹⁷ Based on these simulations, a meta-atom

library was established to fulfill the required phase distribution of the metalens.

The design of the metalens then becomes straightforward. Specifically, the detailed layout of the metasurface is realized by assigning, at each location in the phase map [Fig. 2(a)], a pillar from the library that provides the required phase shift. This one-to-one correspondence enables a direct translation of the desired phase distribution into a physical layout of square pillars with different widths.

The focusing performance of the designed metalens was simulated in 2D using COMSOL. As shown in Fig. 3, the results demonstrate clear focusing behavior, with a focal region spanning from 5110 to 5170 μm . The intended antenna position at 5115 μm lies within this region. Further simulation details are provided in [supplementary material 2](#).

The metalens was fabricated on a double-side polished silicon wafer (515 μm thick). All silicon components, including the spacer and HEB chip, were high-resistivity ($\geq 5 \text{ k}\Omega\cdot\text{cm}$). To fabricate the metalens, a laser writer was used for lithography to define the etching mask pattern of square pillars. Deep reactive ion etching (DRIE) using a Bosch process in an induction-coupled plasma-reactive ion etching (ICP-RIE) system was then applied to etch the silicon and form pillars with heights ranging from 110 to 141 μm , depending on the pillar width, as documented in Fig. 2(c). The change in pillar height arises

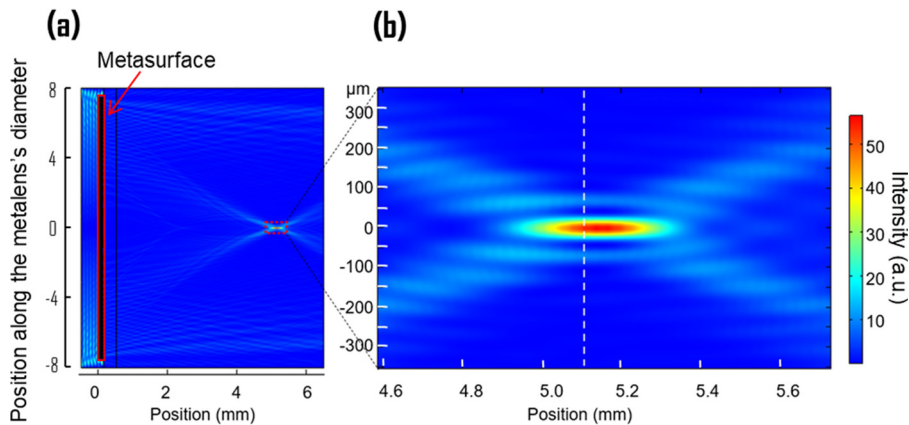


FIG. 3. Electric field intensity distribution of the metalens at 1.63 THz, obtained using a modified 2D simulation approach. (a) Cross-sectional view along the optical axis, showing clear focusing behavior with a well-defined focal spot. (b) Zoomed-in view of the focal region from (a). The focal region spans from 5110 to 5170 μm , with the antenna position at 5115 μm (indicated by the white dashed line) lying within it.

from the loading effect during the etching process.²⁵ A uniform pillar height could be achieved by introducing an etch-stop layer.

Figure 2(e) shows an optical micrograph of the fabricated Si metalens, with the inset providing a zoomed-in image. The pillar sizes deviate from nominal values with an error less than 5%, demonstrating-pattern transfer with high spatial fidelity. Figure 2(f) presents a cross-sectional SEM image, revealing well-defined, high-aspect-ratio pillars and clearly illustrating the loading effect.

To realize the metalens-coupled HEB mixer (in Fig. 1), we used a spiral antenna-coupled NbN HEB mixer chip, which is very well characterized, as described in Ref. 4. We also employed a disc-shaped Si spacer, comparable in surface quality and dimensional accuracy to a conventional Si lens.¹⁰ The spacer is mounted in the same mixer block used for elliptical Si lenses (a “diameter” of 10 mm)⁴ and is designed for cryogenic operation.

The metalens sample (labeled as “DMLv9_03”) was aligned and glued to the front surface of the spacer (\varnothing (diameter) = 10 mm), while the HEB chip was aligned and glued to the back surface (\varnothing = 8.9 mm). Using the technique in Ref. 10, the alignment accuracy of both components relative to the spacer’s optical axis was within 3 μm .

To evaluate the metalens performance, we conducted heterodyne measurements to determine the double-sideband (DSB) receiver noise temperature ($T_{\text{rec}}^{\text{DSB}}$) of the mixer, which is a figure of merit for a heterodyne receiver. The measurements were performed at 4.4 K using a 1.63 THz line from a far-infrared gas laser as the local oscillator (LO).

A hot (295 K) and cold (77 K) blackbody load was alternately placed in front of the receiver. The experimental setup was identical to that used in our previous lens-HEB mixer study and is given in [supplementary material 3](#).⁴

The THz signal from the blackbody passed through air, a 3 μm Mylar beam splitter, an ultra-high molecular weight polyethylene window at 295 K, a low pass filter with a cutoff frequency of 5.8 THz at 4 K (heat filter), and finally the metalens, which focused the beam onto the spiral antenna. The resulting intermediate frequency (IF) signal, produced by mixing the blackbody radiation and LO, was routed through a circulator, amplified by a low-noise SiGe amplifier (LNA) at 4.2 K, filtered at 1.7 GHz with an 80 MHz bandwidth, and further amplified by a room-temperature LNA to produce the receiver output power.

The receiver output power, P_{hot} and P_{cold} , measured when the mixer is exposed to hot and cold blackbody loads, respectively, is recorded as a function of HEB current (by varying the LO power) at an optimal bias voltage of 0.6 mV, as shown in Fig. 4(a). Using the standard Y-factor method and the Callen–Welton formula for effective blackbody temperatures,^{1,2} $T_{\text{rec}}^{\text{DSB}}$ is derived from the measured P_{hot} and P_{cold} , and also plotted in the same figure.

The minimum $T_{\text{rec}}^{\text{DSB}}$ is 1794 K, recorded at a mixer current of 41.5 μA . For comparison, the state-of-the-art $T_{\text{rec}}^{\text{DSB}}$ using an AR-coated elliptical lens–spiral NbN HEB mixer at 1.63 THz is 530 K.⁴ Notably, the value of 1794 K already surpasses the performance reported in Ref. 26, which marked one of the earliest demonstrations of lens–antenna NbN

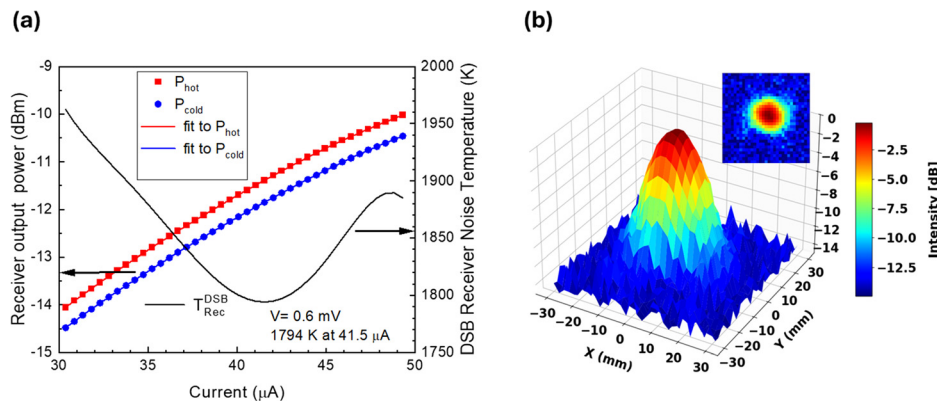


FIG. 4. (a) DSB receiver noise temperature $T_{\text{rec}}^{\text{DSB}}$ of the metalens-coupled HEB mixer measured at 4.4 K and 1.63 THz. The values are extracted from measured receiver output power vs HEB bias current in response to a hot load (P_{hot}) or a cold load (P_{cold}). Both measured data and fitted curves are shown. (b) Far-field beam profile of the metalens-coupled HEB mixer, measured at a distance of 450 mm from the metasurface. The 3D profile is shown on a dB scale; the corresponding 2D beam pattern is shown in the inset.

HEB mixers. The measured T_{rec}^{DSB} includes contributions from the mixer itself, as well as optical losses and noise introduced by components in front of the mixer and by the metalens. These contributions are described by Eq. (2), derived from Refs. 2 and 5,

$$T_{rec}^{DSB} = T_{opt} + \frac{T_{lens}}{G_{opt}} + \frac{T_{mixer}^{DSB}}{G_{opt}G_{lens}} + \frac{T_{IF}}{G_{opt}G_{lens}G_{mixer}^{DSB}}, \quad (2)$$

where T_{opt} is the noise temperature contribution from the optical components in front of the metalens ($=101$ K), T_{mixer}^{DSB} is the mixer noise temperature, G_{mixer}^{DSB} is the mixer gain, G_{opt} is the total optical gain of the components before the lens, G_{lens} is the optical gain of the metalens or the power coupling efficiency, T_{lens} is the noise temperature contribution from the metalens, which equals $\left(\frac{1}{G_{lens}} - 1\right) \times T_{CW,(4K)}$, where $T_{CW,(4K)}$ ($=39.1$ K) is a Callen–Welton temperature,^{2,5} and T_{IF} the noise temperature of the IF chain ($=6.5$ K). The measured T_{rec}^{DSB} can thus be used to extract the power coupling efficiency of the metalens.

To estimate G_{lens} , we use Eq. (2) along with the following parameters from Ref. 4: $T_{mixer}^{DSB} = 217$ K and $G_{mixer}^{DSB} = -4.0$ dB. These values were obtained using the same HEB chip mounted behind an AR-coated Si lens at 1.63 THz, with the lens contribution removed. We also adopt $G_{opt} = -2.25$ dB from Ref. 4, as the measurement setup was identical. From this, we determine $G_{lens} = -5.9$ dB, corresponding to a power coupling efficiency of 26%.

A more direct and reliable estimation of G_{lens} can be obtained by measuring the total receiver gain G_{total} using the U-factor method.²⁸ The U-factor is defined as the ratio of the receiver output power at optimal operating conditions (where $T_{rec}^{DSB} = 1794$ K) to the output power when the HEB is in the superconducting state and illuminated by the hot load. G_{total} is then derived from the U-factor using the following expression [Eq. (3)], as given in Ref. 27:

$$G_{total} = \frac{U(T_{IF} + T_{ref})}{T_{rec}^{DSB} + T_{293K}}, \quad (3)$$

where T_{ref} equals 4.2 K, which is the physical temperature of the 50 Ω resistor terminating the circulator.

Using the measured U-factor of 10.48 dB and Eq. (3), G_{total} is calculated to be -12.35 dB. Since $G_{total} = G_{opt}G_{lens}G_{mixer}^{DSB}$, we derive $G_{lens} = -6.1$ dB or 25% using the same G_{mixer}^{DSB} and G_{opt} values as before [when applying Eq. (2)]. Both methods yield consistent values for G_{lens} , confirming the reliability of our measurements. This 25% lens efficiency corresponds to 27% of that of the AR-coated Si lens. The latter is based on a simulation.

We now discuss the implications of the measured optical gain of the metalens. G_{lens} can be decomposed into two components: the focusing efficiency of the metalens and the beam-mode matching efficiency between the focused beam and the antenna. Previous studies report a focusing efficiency of $\sim 46\%$ ¹⁹ for an all-Si metalens, assuming no reflection losses at the air–Si interface. Given our measured G_{lens} of 25%, the beam-mode matching efficiency is estimated to be $\sim 54\%$. This value is close to the truncation efficiency of $\sim 53\%$, calculated from the radiation pattern of the spiral antenna and the diameter of the metalens, implying our low beam-mode matching is dominated by the truncation.

To improve beam-mode matching efficiency, we need to increase the lens diameter or NA. More importantly, a new metalens design

should also adopt a phase profile derived directly from the beam of the spiral antenna used in the mixer.

The next step is to improve the focusing efficiency. We need to design a metalens by reducing the losses from unwanted diffraction orders that fundamentally limit focusing efficiency.²² Recent work has shown that inverse-designed pillar shapes can overcome this, achieving focusing efficiencies up to $\sim 90\%$ at infrared wavelengths.²⁹ This method allows direct control over structural complexity via Fourier decomposition of the surface gradient. Additionally, an AR structure could be introduced to reduce a $\sim 15\%$ reflection loss at the air–Si metasurface interface.³⁰ The AR structure can further improve the focusing efficiency. The ultimate goal is to raise G_{lens} above 70%, which should be feasible and would substantially enhance the observing efficiency of an array relative to a single-pixel receiver.⁵

We now briefly address two other characteristics of the metalens: far-field beam pattern and bandwidth. Using the heterodyne beam measurement setup in Ref. 28, we measured the far-field beam pattern of the mixer in the x–y plane at a distance of 450 mm from the metasurface. As shown in Fig. 4(b), the beam exhibits a Gaussian-like profile. No sidelobes were observed above -14 dB relative to the main peak, limited by the noise floor of the measurement system, which is approximately -14 dB. The absence of sidelobes confirms the good Gaussian character of the metalens–antenna HEB mixer. The 2D inset in Fig. 4(b) shows an elliptical beam profile, attributed to the asymmetric geometry of the spiral antenna.

Our metalens is expected to have a bandwidth of ~ 80 GHz, which is derived by a simulation of the focused beam in 2D as a function of frequency, centered at 1.63 THz, and which is taken when the intensity at the focusing plane decreased by roughly 3 dB. In contrast, the elliptical lens has a wide bandwidth (~ 4 THz), as demonstrated, e.g., in Ref. 4.

In summary, we demonstrate an all-Si metalens that couples free-space THz radiation to a spiral antenna-coupled NbN HEB mixer at 1.63 THz. The receiver achieves a competitive DSB receiver noise temperature of 1800 K and exhibits a Gaussian-like far-field beam with sidelobes below -14 dB. Using standard heterodyne techniques, we accurately determine the metalens power coupling efficiency to be 25%. Pathways for further improvement are identified. This metalens–antenna mixer serves as a promising pathfinder for scalable HEB focal plane arrays in future space observatories.

See the [supplementary material](#) for the following: [supplementary material 1](#): An aluminum mixer block that holds the metalens–spacer–HEB unit, mounted on the 4 K cold plate of a cryostat. [Supplementary material 2](#): A two-dimensional simulation of the focused beam for the metalens using COMSOL Multiphysics®. [Supplementary material 3](#): A schematic view and a photo of the heterodyne measurement setup used to characterize the metalens–HEB mixer at 1.63 THz.

This work was supported by the Horizon Europe Radioblocks project (Grant No. 101093934) and the TU Delft Space Institute. The authors thank Behnam Mirzaei for fabricating the HEB, Qing Yu for sharing expertise on metalens design, Shahab Dabironezare for valuable discussions on the antenna, Vishal Anvekar for the optical micrograph of the metalens, Wouter Laauwen and Willem Jan Vreeling for their support with the measurements, and Damian Audley for English proofreading the manuscript.

AUTHOR DECLARATIONS

Conflict of Interest

The authors have no conflicts to disclose.

Author Contributions

D. Ren: Conceptualization (equal); Data curation (equal); Formal analysis (equal); Investigation (equal); Writing – original draft (equal). **J. R. G. Silva:** Data curation (equal); Formal analysis (equal); Writing – review & editing (equal). **S. Cremasco:** Data curation (equal); Formal analysis (equal). **Z. Zhao:** Data curation (equal); Formal analysis (equal). **W. Ji:** Formal analysis (equal). **J. de Graaff:** Formal analysis (equal). **A. J. L. Adam:** Conceptualization (equal); Supervision (equal); Writing – review & editing (equal). **J. R. Gao:** Conceptualization (equal); Funding acquisition (equal); Project administration (equal); Supervision (equal); Writing – review & editing (equal).

DATA AVAILABILITY

The data that support the findings of this study are available from the corresponding author upon reasonable request.

REFERENCES

- ¹J. Zmuidzinas and P. L. Richards, “Superconducting detectors and mixers for millimeter and submillimeter astrophysics,” *Proc. IEEE* **92**, 1597 (2004).
- ²H.-W. Hubers, “Terahertz heterodyne receivers,” *IEEE J. Select. Top. Quantum Electron.* **14**, 378 (2008).
- ³W. Zhang, P. Khosropanah, J. R. Gao, E. L. Kollberg, K. S. Yngvesson, T. Bansal, R. Barends, and T. M. Klapwijk, “Quantum noise in a terahertz hot electron bolometer mixer,” *Appl. Phys. Lett.* **96**, 111113 (2010).
- ⁴B. Mirzaei, J. R. G. Silva, W.-J. Vreeling, W. M. Laauwen, D. Ren, and J.-R. Gao, “Reduced noise temperatures of a THz NbN hot electron bolometer mixer,” *IEEE Trans. Terahertz Sci. Technol.* **15**(1), 91–99 (2025).
- ⁵C. K. Walker, *Terahertz Astronomy* (Taylor & Francis, New York, NY, 2016).
- ⁶S. Cherednichenko, V. Drakinskiy, T. Berg, P. Khosropanah, and E. Kollberg, “Hot-electron bolometer terahertz mixers for the Herschel Space Observatory,” *Rev. Sci. Instrum.* **79**, 034501 (2008).
- ⁷C. Risacher, R. Güsten, J. Stutzki, H.-W. Hübers, R. Aladro, A. Bell, C. Buchbender, D. Büchel, T. Csengeri, C. Duran, U. U. Graf, R. D. Higgins, C. E. Honingh, K. Jacobs, M. Justen, B. Klein, M. Mertens, Y. Okada, A. Parikka, P. Pütz, N. Reyes, H. Richter, O. Ricken, D. Riquelme, N. Rothbart, N. Schneider, R. Simon, M. Wienold, H. Wiesemeyer, M. Ziebart, P. Fusco, S. Rosner, and B. Wohler, “The upGREAT dual frequency heterodyne arrays for SOFIA,” *J. Astron. Instrum.* **7**, 1840014 (2018).
- ⁸Y. M. Seo, P. F. Goldsmith, C. K. Walker, D. J. Hollenbach, M. G. Wolfire, C. A. Kulesa, V. Tolls, P. N. Bernasconi, Ü. Kavak, F. F. S. Van Der Tak, R. Shipman, J. R. Gao, A. Tielens, M. G. Burton, H. Yorke, E. Young, W. L. Peters, A. Young, C. Gropi, K. Davis, J. L. Pineda, W. D. Langer, J. H. Kawamura, A. Stark, G. Melnick, D. Rebolledo, G. F. Wong, S. Horiuchi, and T. B. Kuiper, “Probing ISM structure in Trumpler 14 and Carina I using the stratospheric terahertz observatory 2,” *Astrophys. J.* **878**, 120 (2019).
- ⁹J. R. G. Silva, W. M. Laauwen, B. Mirzaei, N. Vercruyssen, M. Finkel, M. Westerveld, N. More, V. Silva, A. Young, C. Kulesa, C. Walker, F. Van Der Tak, and J. R. Gao, “ 4×2 Hot electron bolometer mixer arrays for detection at 1.4, 1.9, and 4.7 THz for the balloon-borne terahertz observatory GUSTO,” *J. Astron. Telesc. Instrum. Syst.* **11**, 016001 (2025).
- ¹⁰J. R. G. Silva, M. Finkel, W. M. Laauwen, M. Westerweld, N. More, A. Young, C. Kulesa, C. Walker, F. Van Der Tak, and J. R. Gao, “High accuracy pointing for quasi-optical THz mixer arrays,” *IEEE Trans. Terahertz Sci. Technol.* **12**, 53 (2022).
- ¹¹S. Zhang, A. Soibel, S. A. Keo, D. Wilson, S. Rafol, D. Z. Ting, A. She, S. D. Gunapala, and F. Capasso, “Solid-immersion metalenses for infrared focal plane arrays,” *Appl. Phys. Lett.* **113**, 111104 (2018).
- ¹²N. Yu, P. Genevet, M. A. Kats, F. Aieta, J.-P. Tetienne, F. Capasso, and Z. Gaburro, “Light propagation with phase discontinuities: generalized laws of reflection and refraction,” *Science* **334**(6054), 333 (2011).
- ¹³X. Zang, B. Yao, L. Chen, J. Xie, X. Guo, A. V. Balakin, A. P. Shkurinov, and S. Zhuang, “Metasurfaces for manipulating terahertz waves,” *Light: Adv. Manuf.* **2**, 148 (2021).
- ¹⁴F. Zhao, X. Jing, and M. Yu, “Research progress on the principle and application of metalenses based on metasurfaces,” *J. Appl. Phys.* **137**, 050701 (2025).
- ¹⁵S. V. Hum and J. P. Perruisseau-Carrier, “Reconfigurable reflectarrays and array lenses for dynamic antenna beam control: A review,” *IEEE Trans. Antennas Propag.* **62**, 183 (2014).
- ¹⁶C.-C. Chang, D. Headland, D. Abbott, W. Withayachumnankul, and H.-T. Chen, “Demonstration of a highly efficient terahertz flat lens employing tri-layer metasurfaces,” *Opt. Lett.* **42**, 1867 (2017).
- ¹⁷M. Yang, X. Shen, Z. Li, Z. Wen, G. Chen, Z. Zhang, G. Liang, H. Li, and Z. Shang, “High focusing efficiency metalens with large numerical aperture at terahertz frequency,” *Opt. Lett.* **48**, 4677 (2023).
- ¹⁸Q. Yang, S. Kruk, Y. Xu, Q. Wang, Y. K. Srivastava, K. Koshelev, I. Kravchenko, R. Singh, J. Han, Y. Kivshar, and I. Shadrivov, “Mie-resonant membrane huygens’ metasurfaces,” *Adv. Funct. Mater.* **30**, 1906851 (2020).
- ¹⁹H. Zhang, X. Zhang, Q. Xu, C. Tian, Q. Wang, Y. Xu, Y. Li, J. Gu, Z. Tian, C. Ouyang, X. Zhang, C. Hu, J. Han, and W. Zhang, “High-efficiency dielectric metasurfaces for polarization-dependent terahertz wavefront manipulation,” *Adv. Opt. Mater.* **6**, 1700773 (2018).
- ²⁰Q. Yu, K. He, X. Wu, J. Liu, and W. Chen, “Design of flat all-dielectric metasurface lens for antenna-coupled transition-edge sensor bolometers,” *J. Low Temp. Phys.* **214**, 92 (2024).
- ²¹H. Pang, S. Yin, Q. Deng, Q. Qiu, and C. Du, “A novel method for the design of diffractive optical elements based on the Rayleigh–Sommerfeld integral,” *Opt. Lasers Eng.* **70**, 38 (2015).
- ²²R. Menon and B. Sensale-Rodriguez, “Inconsistencies of metalens performance and comparison with conventional diffractive optics,” *Nat. Photonics* **17**, 923 (2023).
- ²³E. V. Loewenstein, D. R. Smith, and R. L. Morgan, “Optical constants of far infrared materials 2: Crystalline solids,” *Appl. Opt.* **12**, 398 (1973).
- ²⁴M. Pan, Y. Fu, M. Zheng, H. Chen, Y. Zang, H. Duan, Q. Li, M. Qiu, and Y. Hu, “Dielectric metalens for miniaturized imaging systems: Progress and challenges,” *Light: Sci. Appl.* **11**, 195 (2022).
- ²⁵B. Horstmann, D. Pate, B. Smith, M. A. Mamun, G. Atkinson, Ü. Özgür, and V. Avrutin, “Cryogenic DRIE processes for high-precision silicon etching in MEMS applications,” *J. Micromech. Microeng.* **34**, 075008 (2024).
- ²⁶A. D. Semenov, H.-W. Hübers, J. Schubert, G. N. Gol’tsman, A. I. Elantiev, B. M. Voronov, and E. M. Gershenzon, “Design and performance of the lattice-cooled hot-electron terahertz mixer,” *J. Appl. Phys.* **88**, 6758 (2000).
- ²⁷S. Cherednichenko, M. Kroug, H. Merkel, P. Khosropanah, A. Adam, E. Kollberg, D. Loudkov, G. Gol’tsman, B. Voronov, H. Richter, and H.-W. Huebers, “1.6 THz heterodyne receiver for the far infrared space telescope,” *Phys. C* **372–376**, 427 (2002).
- ²⁸J. R. G. Silva, M. Finkel, W. M. Laauwen, S. J. C. Yates, B. Mirzaei, N. Vercruyssen, A. Young, C. Kulesa, C. Walker, F. Van Der Tak, and J. R. Gao, “Beam waist properties of spiral antenna coupled HEB mixers at supra-THz frequencies,” *IEEE Trans. Terahertz Sci. Technol.* **13**, 167 (2023).
- ²⁹P. Dainese, L. Marra, D. Cassara, A. Portes, J. Oh, J. Yang, A. Palmieri, J. R. Rodrigues, A. H. Dorrah, and F. Capasso, “Shape optimization for high efficiency metasurfaces: Theory and implementation,” *Light: Sci. Appl.* **13**, 300 (2024).
- ³⁰Z. Zhao, D. Ren, S. Cremasco, J. R. G. Silva, A. J. L. Adam, and J. R. Gao, “Anti-reflection structure for a silicon metalens at 1.6 THz,” in *34th IEEE International Symposium on Space THz Technology (ISSTT 2025)* (IEEE, Berlin, Germany, 2025).